Available online at www.sciencedirect.com
SCIENCE DIRECT®
Journal of Nuclear Materials 337–339 (2005) 347–351
journal of nuclear materials
www.elsevier.com/locate/jnucmat

Statistical analysis of turbulent front propagation in the scrape-off-layer

Ph. Ghendrih [a,*], Y. Sarazin [a], G. Attuel [a], S. Benkadda [b], P. Beyer [b], G. Darmet [a], G. Falchetto [a], C. Figarella [a], X. Garbet [a], V. Grandgirard [a], M. Ottaviani [a]

[a] *Association Euratom-CEA, DRFC/DSM/CEA Cadarache, 13108 St Paul lez Durance, cédex, France*
[b] *PIIM, CNRS-Université de Provence, 13397 Marseille, France*

Abstract

The intermittent transport in the SOL is analysed in terms of the interaction between the average profile and the population of large transport events, the fronts. This provides the basis for the statistical analysis presented in this paper. Data from 2D numerical simulations is analysed here. The mean density e-folding length for the fronts is observed to be the same as that of the time average profile. The mean ballistic velocity of the fronts has a radial Mach number of 0.03. A symmetric distribution of poloidal Mach numbers is found, its width is comparable to that of the radial Mach number, $\Delta M \sim 0.02$. The small fronts are found to be isotropic, the larger fronts are elongated radially (aspect ratio ~ 6). A characteristic poloidal scale is found, typically 7 Larmor radii.

PACS: 05.60.+w; 52.25.Fi; 52.35.Ra
Keywords: SOL transport; Plasma turbulence; Intermittent transport; Particle flux; Simulation

1. Introduction

A proper understanding of cross-field transport is most important since the balance between cross-field and parallel transport are key aspects in the scrape-off-layer of magnetically confined plasmas [1]. The impact for a next step device addresses issues such as transport to the main chamber wall and consequently reduced performance of the divertor in terms of particle control (main species and impurities) and uncertainty in the modelling effort since the latter is based on diffusive transport. Recent theoretical [2,3] and experimental [4,5] investigation of turbulent transport has indicated that a significant fraction of the particle outflux was transported by large intermittent events. The analysis of the experimental data has led to a statistical description of these events including the radial profiles of the radial velocity and particle content of such intermittent events [4,5]. Imaging of the turbulence allows one to observe front propagation, usually in 2D, with complex trajectories. The goal here is to quantify this information in order to improve the description of the intermittent transport and to establish common tools and criteria to compare experimental and theoretical results. Control of this SOL turbulence with a biased ring is investigated in [6].

* Corresponding author.
E-mail address: philippe.ghendrih@cea.fr (Ph. Ghendrih).

0022-3115/$ - see front matter © 2004 Elsevier B.V. All rights reserved.
doi:10.1016/j.jnucmat.2004.10.068

We address SOL transport with simulations of the SOL interchange instability [7,8]. We restrict the analysis to the density at constant temperature in the cold ion limit. The system is governed by two equations, one for the normalised density field and the other for the normalised electric potential. The flute assumption allows one to simplify the parallel transport which then takes the form of the loss terms at the sheath. The equations and parameter values will be found in Refs. [2,3,6]. Space is normalised to the hybrid Larmor radius ρ_s, $\rho_s^2 = T_e/m_i$ (T_e is the electron temperature and m_i is the ion mass ratio), time to the ion cyclotron frequency $1/\Omega_i$ and velocity to the sound velocity, $c_s = \rho_s\Omega_i$. Ballistic propagation velocities (velocity v) are thus directly computed as Mach numbers $M = v/c_s$. Although very simplified, this system, when flux driven, appears to be generic of SOL transport [9]. (The equations will be found in Appendix A).

2. Interplay between density fronts and the average density

Let us consider the radial particle flux Γ_r at a given position. The time trace exhibits large peaks of positive values (outflux) as well as a background level of small magnitude negative values (influx). The probability distribution function (PDF) $P_r(\Gamma)$ allows one to recover this description. There is a nearly symmetric bulk of particle flux events with negative and positive values, $\Gamma_r/\langle\Gamma_r\rangle$ typically ranging from −7.5 to 7.5, Fig. 1. $\langle\Gamma_r\rangle$ is the average value, $\langle\Gamma_r\rangle = \int_{-\infty}^{+\infty} d\Gamma_r P_r(\Gamma_r)\Gamma_r(r,\theta)$, $\langle\Gamma_r\rangle = 0.0266$. The PDF $P_r(\Gamma)$ is also characterised by a heavy tail towards the positive flux values with a decay that can be fitted by $P_r(\Gamma) \approx P_0\exp(-\Gamma/\Gamma^*)$ with $\Gamma^*/\langle\Gamma_r\rangle \sim 4.252$. The most probable flux value is negative and comparable in magnitude to the average flux $\Gamma_{Pmax}/\langle\Gamma_r\rangle \sim -0.418$. A measure of the weight of the rare events in the transport properties is provided by computing their contribution to the average flux $\Gamma_{PDF}(\Gamma)$ versus their weight in the PDF, $W_{PDF}(\Gamma)$, given by, $\Gamma_{PDF}(\Gamma) = \int_\Gamma^{+\infty} d\Gamma_r P_r(\Gamma_r)\Gamma_r(r,\theta)$ and $W_{PDF}(\Gamma) = \int_\Gamma^{+\infty} d\Gamma_r P_r(\Gamma_r)$, Fig. 2. In the heavy tail region of the PDF, one readily finds the approximate relation $\Gamma_{PDF}(\Gamma) \approx W_{PDF}(\Gamma)(\Gamma + \Gamma^*)$. The function $\Gamma_{PDF}(\Gamma)$ first increases with W_{PDF}, levels off when the negative values of Γ are reached and then decreases to $\langle\Gamma_r\rangle$ as $W_{PDF} \to 1$. This analysis provides a description of the turbulent transport in terms of three fields, the average field, the large magnitude fluctuations in the heavy tail of the PDF and the small magnitude fluctuations. The large magnitude fluctuations are identified as fronts and extend to the fluctuation level such that $\Gamma_{PDF}(\Gamma_{Fronts}) = 1$. For the data used in Fig. 1 this corresponds to $W_{PDF}(\Gamma_{Fronts}) \approx 11.5\%$. In practise, the fronts are defined as the sets of points such that the density locally exceeds twice the average density. These points cluster in structures that represent about 10% of the box size.

3. Characteristic features of a density front

Let us consider a given front, Fig. 3. The radial extent of this front is $47\rho_s$ and approximate surface $356\rho_s^2$. As a result the average width in the poloidal direction is of $7.6\rho_s$ with a maximum width of $10.5\rho_s$. The poloidal extent of $23\rho_s$, shown on Fig. 3, is thus typically a factor two larger than the actual width of the front. It is due to the 'wiggles' of the front in the poloidal direction. The front thus appears to be elongated in the radial direction and exhibits wiggles in the poloidal direction with displacements of the same order as the front width. The density profile in the front follows the curvilinear abscissa s_F of the line of points (r_F,θ_F) such that θ_F is located at the local density maximum for each value r_F. The density profile shown on Fig. 4 is characteristic of a front, there is a nearly constant density in the bulk of the front and a steep density gradient (negative) at the forefront. The profile at given y exhibits multiple peaks that reproduce multiple intersections with the

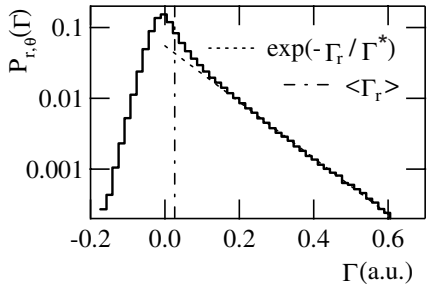

Fig. 1. PDF of the particle flux, the dot-dash line indicates the mean value.

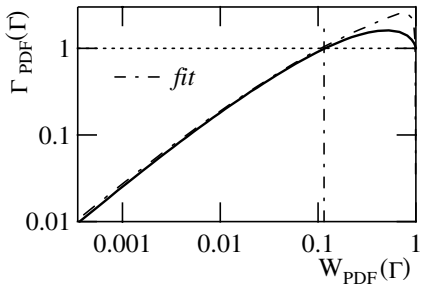

Fig. 2. Contribution of the flux events to the mean flux, Γ_{PDF}, versus weight in the PDF, W_{PDF}.

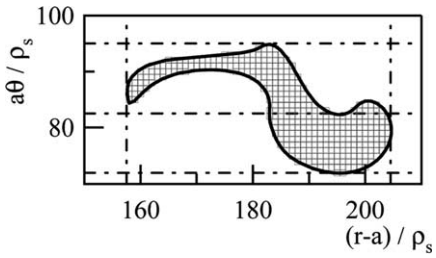

Fig. 3. Front extent at a given time in the (r,θ) plane, radial extent $\sim 47\rho_s$, poloidal width of the shape $\sim 23\rho_s$, although the effective extent is about half (see the dashed lines).

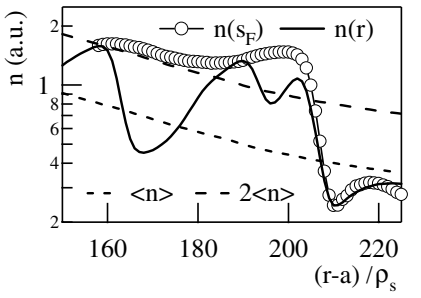

Fig. 4. Density profile in a front, following the line of maximum density $n(s_F)$, radial profile $n(r)$ and time average profile $\langle n \rangle$.

given front as well as crossing the neighbourhood at lower density.

On Fig. 5 are plotted the front density profiles at four different times. The point of the front at largest radial position, labelled FF (Forefront), stands at the intersection of the strong density gradient at the forefront, with the line at twice the average density profile, $n_{FF} = 2\langle n(r_{FF})\rangle$. For the data shown on Fig. 5, one finds a $20\rho_s$ radial shift of FF, for a time step of $600/\Omega_i$. The velocity of the forefront is then found to be $\sim 0.03 c_s$. The front at two different times is plotted on the same curve after shifting FF at the earlier time to the radial and density value of FF at the later time. The shape of the front is hardly changed. The ratio of the front density on the flat top to the average density is nearly constant ~ 3.3. The density gradient at the forefront is unchanged, $n/\nabla n \sim 4.6\rho_s$. Finally, the radial extent of the front is also found to be the same, $L_r \sim 40\rho_s$.

4. Statistical features of density fronts

The statistical properties of the density fronts are analysed according to the features described in Section 3. In particular, the ratio of the density on the flat top of the front to the average density profile is observed to be constant. This property also means that the e-folding length of the front density is comparable to the e-folding length of the average density profile. This is confirmed by the statistics, Fig. 6. The common e-folding length is typically $56\rho_s$. This property is in agreement with experimental observations [3]. The PDF of the e-folding length of the front is found to be nearly Gaussian with a width of $20\rho_s$.

When analysing a given front in Section 3, several values of the radial velocity can be found. In particular, the various points belonging to the front will contribute to the average velocity of the front, but also to changes in the front boundary as well as to particle circulation within the front. Here, the statistical analysis is performed with the velocity of the mass centre of the front. The PDF of the poloidal velocity is very close to symmetric, hence $\langle M_\theta \rangle \sim 0$. In contrast, the PDF of the radial velocity is found to peak at a Mach number $M_r = v_r/c_s \sim 0.03$. The widths of the two distributions are comparable $\Delta M_r \sim \Delta M_\theta \sim 0.02$. The radial dependence of the Mach numbers can be analysed in terms of the profiles of the mean values computed with the PDFs, $\langle M_r \rangle$ and $\langle |M_\theta| \rangle$, Fig. 7. Three regions characterise these profiles, a first region in the vicinity of the separatrix, of width $\sim 30\rho_s$, where the Mach numbers

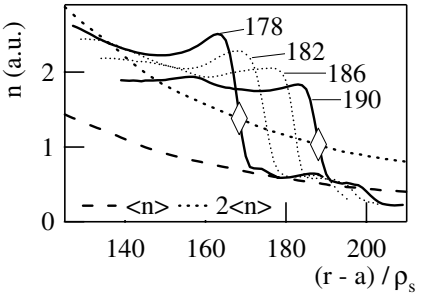

Fig. 5. Density front at 4 different times, 178, 182, 186 and 190 in units $50/\Omega_i$. The two diamonds locate the front head at two times (178 and 190).

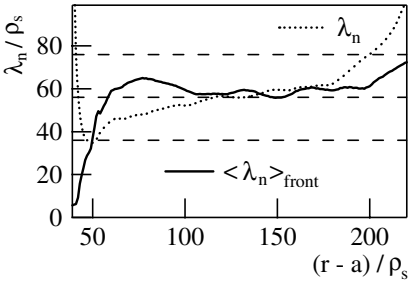

Fig. 6. Profile of the density e-folding length for the time average density λ_n and mean value for the front population $\langle \lambda_n \rangle$. The dashed lines indicate approximately the profile average values of $\langle \lambda_n \rangle$ and width of its PDF.

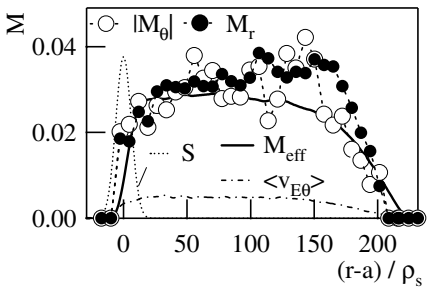

Fig. 7. Profile of the Mach numbers, front population M_r and $|M_\theta|$, and time averaged values, $M_{eff} = \langle \Gamma_r \rangle / \langle n \rangle$ and poloidal drift velocity $\langle v_{E\theta} \rangle$. The three latter are multiplied by 2.5. The source S locates the separatrix.

increase rapidly as the fronts build-up, a second region where the Mach numbers are nearly constant, and a third region towards the stable region of the simulation where the Mach numbers decrease. On Fig. 8, the Mach numbers of the fronts are compared to the profiles of the average fields, the effective Mach number, $M_{eff} = \langle \Gamma_r \rangle_t / \langle n \rangle_t$ and the average zonal flow $\langle |v_{E\theta}| \rangle_t$ (v_E is the electric drift velocity). The radial Mach number averaged on the front population is typically a factor 3 larger than M_{eff}. This underlines the result discussed in Section 2, namely that the large intermittent radial outflux, is partly balanced by a low magnitude influx.

The characteristic scales L_r and L_θ of the fronts appear to be correlated. While L_r varies from 0 to $50\rho_s$ radially L_θ increases from 0 to $25\rho_s$ poloidally. The smaller fronts are found to be isotropic $L_r \sim L_\theta < 10\rho_s$. For larger fronts L_r tends to increase and the poloidal scale of the fronts to level-off at about $10\rho_s$. The PDF of the two scales, Fig. 4, allows one to recover this result. While the PDF of the radial scales does not exhibit a characteristic scale, the poloidal scale is characterised by a peak value at about $7\rho_s$. The occurrence of fronts in the density transport does not appear to be a signature of an inverse cascade in the poloidal direction since the characteristic scales that are reached are similar to

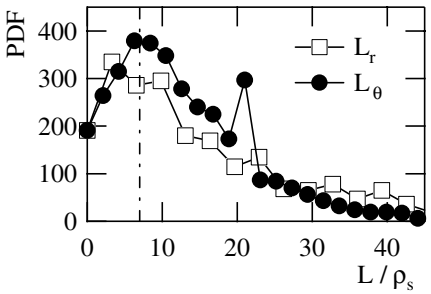

Fig. 8. PDF of the mean extent of the front population restricted to fronts lasting longer than $250/\Omega_i$.

that of the unstable modes in the linear analysis [2]. Some signature on an inverse cascade can be found in the increase of the radial characteristic scale although it appears to level off at values significantly smaller than the system size. Conversely, the splitting of the fronts, that is observed to bound the front life time is reminiscent of a direct cascade with energy transferred to the smaller scales where molecular diffusion erodes away the fronts.

5. Discussion and conclusion

The analysis of the intermittent transport in the SOL indicates that the average field and the fronts exhibit similar e-folding lengths in the radial direction. Furthermore, the fronts are found to predominantly originate in the vicinity of the separatrix where they are rather isotropic. As propagation through the SOL occurs, the fronts extend radially up to four to five times the poloidal scale ($\sim 10\rho_s$). During this phase the radial velocity also increases and reaches a Mach number of the order of 0.03. These features appear to be in qualitative agreement with the experimental observation [3,4]. More quantitative agreement would require an appropriate scan in the simulations to determine the scaling laws that govern these properties.

Very few fronts are found to cross the simulation box in a single ballistic flight. Interaction of the poloidal flows with the fronts appear to strongly bound the lifetime of these events. Indeed shearing of the fronts are observed. They govern the direct cascade to the small scales where molecular diffusion smears out the fronts. The mean poloidal velocity of the mass centre of the fronts is found to be typically one order of magnitude larger that the zonal flows. These poloidal flows on the front scale thus appear to be far more effective in the shearing process of the fronts than the zonal flows. The results presented in this paper indicate that significant interaction is found between the fronts and the background turbulence activity exemplified by the dynamics of the vorticity [9]. The investigation of the dynamics of single transport events [10] falls short of capturing this complex dynamics.

The present analysis of the intermittent SOL turbulence provides a basis to describe the transport properties as resulting from the interaction of three fields, the average field that ultimately is the key quantity in the modelling effort, the fluctuations that do not contribute to transport but that will act as a noise, hereby introducing an appropriate random process, and the large fronts that bear the turbulent transport properties. The statistical results in this paper are a first step in defining the rules of this three field interaction.

Appendix A

Several SOL instabilities are presently investigated (see Refs. [3,10] and the review Ref. [11] for extra references). The model used in the present paper is most effective to investigate generic properties of turbulent transport. We address SOL transport with a very simplified model [2,7,8]. It is based on the interchange instability. We consider particle transport at constant temperature ($T_e \gg T_i$) with fluid equations. The system is governed by two equations, one for the normalised density field $N = n/n_0$, the other for the normalised electric potential $\phi = eU/T_e$.

$$(\partial_t - D\nabla_\perp^2)N + [\phi, N] = -\sigma N e^{(\Lambda-\phi)} + S,$$
$$(\partial_t - \nu\nabla_\perp^2)\nabla_\perp^2\phi + [\phi, \nabla_\perp^2\phi] + g\partial_y \log(N) = \sigma(1 - e^{(\Lambda-\phi)}). \quad (A.1)$$

The diffusion coefficients D and ν are standard collisional particle diffusion and viscosity. The electric drift convection takes the standard form of Poisson brackets $[f, g] = \partial_x f \partial_y g - \partial_y f \partial_x g$, where $x = (r - a)/\rho_s$ is the minor radius normalised by the Larmor radius $\rho_s^2 = T_e/m_i$ and where $y = a\theta/\rho_s$, a is the plasma radius. The interchange destabilising term in the equation for the electric potential is characterised by its magnitude g. The sheath loss terms depend on both the difference between the electric potential and the plasma floating potential and on the sheath conductivity σ [2]. At equilibrium, the particle source term S is then balanced by the end loss term (in the parallel direction). Typical values of the parameters used in the runs will be found in Ref. [3].

References

[1] X. Bonnin et al., these Proceedings. doi:10.1016/j.jnucmat.2004.10.102.
[2] Y. Sarazin, Ph. Ghendrih, Phys. Plasmas 5 (1998) 4214.
[3] Ph. Ghendrih et al., Nucl. Fus. 43 (2003) 1013.
[4] D.L. Rudakov et al., Plasma Phys. Control. Fus. 44 (2002) 717.
[5] J.A. Boedo et al., Phys. Plasmas 10 (2003) 1670.
[6] C. Figarella et al., these Proceedings. doi:10.1016/j.jnucmat.2004.10.069.
[7] A.V. Nedospasov, Sov. J. Plasma Phys. 15 (1989) 659.
[8] X. Garbet et al., Nucl. Fus. 31 (1991) 967.
[9] Y. Sarazin et al., J. Nucl. Mater. 313–316 (2003) 796.
[10] D.A. D'Ippolito, J.R. Myra, S.I. Krasheninnikov, Phys. Plasmas 9 (2002) 222.
[11] B.A. Carreras, these Proceedings. doi:10.1016/j.jnucmat.2004.10.034.